Energy & Environmental Science

Accepted Manuscript

ROYAL SOCIETY OF CHEMISTRY

www.rsc.org/ees

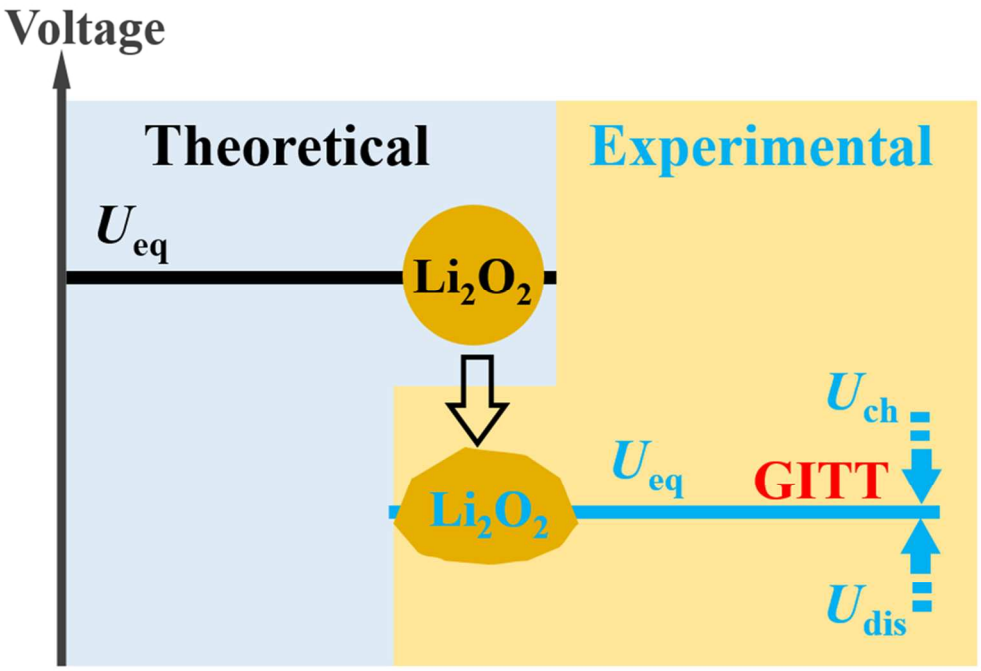

Key thermodynamic and kinetic issues of the Li-O2 battery are studied by GITT technique for the first time.
54x36mm (600 x 600 DPI)

Journal Name

RSCPublishing

COMMUNICATION

Equilibrium Voltage and Overpotential Variation of Nonaqueous Li-O_2 Batteries Using Galvanostatic Intermittent Titration Technique

Cite this: DOI: 10.1039/x0xx00000x

Received 00th January 2012,
Accepted 00th January 2012

DOI: 10.1039/x0xx00000x

www.rsc.org/

Z. H. Cui,[a] X. X. Guo[a,]* and H. Li[b]

The Li-air (or Li-O_2) battery offers great potential for achieving much higher specific gravimetric energy density than start-of-the-art Li-ion batteries. It has become the focus in field of scientific research especially in the past several years.[1-6] By virtue of material design of the air cathodes, introduction of redox mediator, optimization of operation protocols, and adding the soluble catalyst in the electrolyte, many reports showed that the Li-O_2 batteries could run for hundred or even thousand cycles with delivering considerably great specific capacities.[7-16] In spite of rapid progress on improving cyclic performance and reducing voltage polarization, many issues on thermodynamics and kinetics in nonaqueous Li-O_2 batteries are still not very clear.

The forward discharging reaction and backward charging reaction of lithium and oxygen in air cathode can be written as the following:

$$2Li^+ + 2e^- + O_2 \leftrightarrow Li_2O_2 \quad (1)$$

According to the formation energies of the reactants and products at 25°C under ambient condition, the thermodynamic equilibrium voltage (emf) for the reaction (1) in aprotic electrolyte is 2.959 V vs Li^+/Li.[1,17] Based on the surface enhanced Raman spectroscopy and differential electrochemical mass spectroscopy (DEMS) investigations,[18] it is suggested that LiO_2 exists as an intermediate phase and then disproportionates to Li_2O_2, as described by equation (2) and (3):

$$Li^+ + e^- + O_2 \leftrightarrow LiO_2 \quad (2)$$

$$2LiO_2 \leftrightarrow Li_2O_2 + O_2 \quad (3)$$

The emf value for reaction (2) is 3.0 V.[19] The single electron reaction path (2) during discharging was argued by a combination experimental of cyclic voltammetry and DEMS.[20].

During charging, the Li_2O_2 is oxidized directly in a one-step reaction without passing the decomposition of LiO_2.[20] Kang *et al* agreed that the direct decomposition of Li_2O_2 is a thermodynamic equilibrium reaction path, but the formation of a series of off-stoichiometric $Li_{2-x}O_2$ compounds will be favourable for decreasing the overpotential.[21] Above arguments could be clarified by showing open circuit voltage (OCV) profiles. However, experimentally, thermodynamic equilibrium voltages of Li-O_2 batteries during discharging and charging have rarely been measured.

High overpotential of discharging (oxygen reduction reaction: ORR) and charging (oxygen evolution reaction: OER), is actually the most challengeable problem for Li-O_2 batteries, leading to a low round-trip electrical energy efficiency, typically less than 70%.[2] In the best case,[16] the difference in charge and discharge voltage is approximately 0.50-0.75 V. It leads to an electrical energy efficiency of ~75-85%, which is below the value of 90% required by practical applications.[2] Whether this voltage gap can be ultimately removed or decreased significantly needs deep understanding of its thermodynamic and kinetic features.

Broader context

The Li-air (or Li-O_2) battery has attracted wide attention since it has the highest theoretical specific gravimetric energy density. In spite of rapid progress on improving cyclic performance and reducing voltage polarization, many key issues on thermodynamics and kinetics in nonaqueous Li-O_2 batteries are still not very clear. In this report, by using the galvanostatic intermittent titration technique, several novel phenomena are observed, such as zero voltage gap for the open circuit voltage (OCV) between charging and discharging, asymmetrical polarization behaviours at different current densities and temperature, continuous increase of overpotential during charging, negative temperature coefficient of the cell's thermodynamic equilibrium voltage. These results could inspire other researchers to comprehensively investigate the complicated reaction mechanism, thermodynamic and kinetic properties of the Li-air battery as well as other advanced batteries.

Taking into account the electrochemical reactions occurred at the cathode, there should be many factors affecting the cathode reaction rates as well as the overpotentials, at least including Li^+ and O_2 transfer at the gas/electrolyte and electrolyte/cathode interfaces, Li^+, e^- and O^{2-} transport in the lattice of Li_2O_2, nucleation, growth and decomposition of Li_2O_2, and other chemical reactions related to the electrolyte. All these factors contribute to the discharge or charge overpotentials, which can be experimentally determined according to the equation:

$$\boldsymbol{\eta = U_{meas} - U_{eq}} \quad (4)$$

where U_{eq} is the equilibrium voltage and U_{meas} is the experimentally measured voltage for discharge or charge at certain current density. Nevertheless, so far there are few reports on investigation of the U_{eq} and η.[22]

The galvanostatic intermittent titration technique (GITT), which combines transient and steady-state measurements, is a widely used

tool to determine the U_{eq} and η values.[23] In this work, we carry out study on the OCV and overpotential issues of Li-O_2 batteries with intentionally selected N-methyl-N-propylpiperidinium bis(trifluoromethansulfony)imide (PP13TFSI) as the electrolyte solvent. Taking advantage of relatively good chemical and electrochemical stability of this electrolyte at elevated temperature,[24] the values of U_{eq}, discharge overpotential (η_{dis} = U_{dis} - U_{eq}) and charge overpotential (η_{ch} = U_{ch} - U_{eq}) measured with different current densities as well as at different temperatures are determined. Mechanism underlying the electrochemical reactions during cell operations is discussed accordingly.

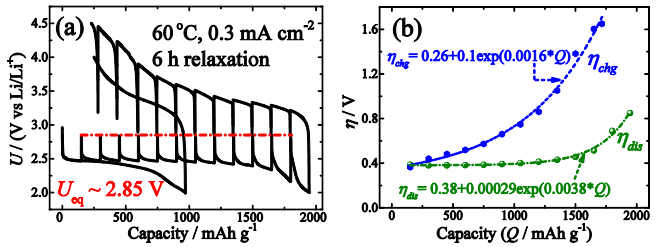

Fig. 1. (a) GITT curves plotted with the voltage as a function of specific capacity. The continuous cycle curve is given for comparison. (b) The overpotential values as a function of capacity. The batteries were measured at 60°C and the fixed current density of 0.3 mA cm^{-2} with the relaxation time of 6 h.

GITT measurements of the Swagelok-type Li-O_2 batteries with PP13TFSI:$LiClO_4$ as the electrolytes and vertical-aligned carbon nanotubes (VACNTs) as the cathodes were carried out. Fig. 1a shows the GITT curves for the battery voltage as a function of specific capacity measured at 60°C and the fixed current density of 0.3 mA cm^{-2} during galvanostatic discharge/charge with the relaxation time of 6h. Correspondingly, Fig. 1b shows η_{dis} as well as η_{ch} as a function of capacity (Q). From the figures, four points are worthwhile noting.

First of all, the discharge capacity under the GITT condition is nearly a factor of two larger than that for the continuous galvanostatic discharge (Fig. 1a). Scanning electron microscopy (SEM) measurement reveals that the Li_2O_2 grows like the abacus balls around the carbon nanotubes at the current density of 0.3 mA cm^{-2} under either GITT or continuous condition (Fig. S1). Nevertheless, the particles in the GITT case are smaller in size (~100 nm) while larger in density than those in the continuous galvanostatic discharge case. The increased density of Li_2O_2 particles indicates that the GITT condition promotes usage of the carbon-nanotube surfaces, leading to the increased discharge capacity. This phenomenon has also been noticed by Zhu et al.[25] In their results, discharging with 120 minutes interval at current density of 0.25 mA cm^{-2} can increase the capacity to 1250 mAh g^{-1} compared to 750 mAh g^{-1} for continuous galvanostatic discharge.

Second of all, in the process of discharge (Fig. 1a), nearly all the OCVs reach the same U_{eq} of 2.85 V after 6 h relaxation. Actually, as shown by GITT curves in Fig. S2, the OCVs during the whole process reach the same value of 2.85 V after 24h relaxation. The equilibrium voltage of an electrochemical reaction is determined by the formation energy difference of the reactants and products, as shown in Nernst Equation (5):[26]

$$\Delta_r G = \sum \Delta_f G_{i(products)} - \sum \Delta_f G_{i(reactants)} = \left(\sum \Delta_f H_{i(products)} - \sum \Delta_f H_{i(reactants)}\right) - T\left(\sum \Delta_f S_{i(products)} - \sum \Delta_f S_{i(reactants)}\right) = -nU_{eq}F \quad (5)$$

where n refers to the number of the charge transferred during the reaction per mole reactant, F is the Faraday constant, ΔH is the enthalpy and ΔS is the entropy of the reaction. U_{eq} varies with temperature, determined by the reaction entropy. A linear relationship between U_{eq} and temperature is measured (Fig. S3). $\Delta_r S$ of the measured Li-O_2 battery is -62.6 (-3.25×10^{-4} nF, with n = 2) J·mol^{-1}·K^{-1}. This negative value is consistent with theoretical expectation. As can be derived from Eq. (5), $U_{eq} = \left[-\left(\Delta H_{Li_2O_2} - 2\Delta H_{Li} - \Delta H_{O_2}\right) + T\left(\Delta S_{Li_2O_2} - 2\Delta S_{Li} - \Delta S_{O_2}\right)\right]/nF$. According to the reference[27], the standard entropy values for Li_2O_2 (solid), Li (solid) and O_2 (gas) are 56.5, 29.1, and 205.1 J·mol^{-1}·K^{-1}, respectively, leading to a negative value of $\Delta_r S$ which equals to -206.8 J·mol^{-1}·K^{-1}. Therefore, the U_{eq} decreases with the increase of the temperature.

According to the results shown in Fig. S3, the simulated U_{eq} at 25°C is 2.861 V. It is interesting to notice that this value is 0.098 V smaller than the theoretical value 2.959 V of the reaction (1). X-ray diffraction (XRD) scans reveal that Li_2O_2 is the only detectable crystalline product in both discharge and charge processes (Fig. S4). Under standard condition, the emf of the reaction (1) should be constant and this value is 2.959 V if the formation energy value from the bulk Li_2O_2 and lithium, and the oxygen partial pressure of 1 atm are taken. In real situation, the formed Li_2O_2 could include two parts, the defective Li_2O_2 nanoparticle and solvated Li_2O_2 in solvents. The solubility of Li_2O_2 in the current electrolyte is not clear. It should be a low value. If the Li_2O_2 is saturated soon after discharging, then variation of the concentration of Li_2O_2 could be negligible. The observed emf value is constant in the most of discharge and charge range, indicating that the solubility of Li_2O_2 should be very small and the concentration of solvated Li_2O_2 in solvents does not change immediately after the discharging. Currently, it is not clear quantitatively whether the solvated Li_2O_2 in solvents is one of the reasons that change the emf value from 2.959 V to 2.85 V. Previous reports indicate that the Li_2O_2 crystals with various orientations and different surface energies might be formed.[22,28] It is known that the variation of the surface energy during discharge and charge may influence emf for conversion reaction.[27] The theoretical emf of 2.959 V is calculated based on thermodynamic data of the homogenous bulk Li_2O_2. Therefore, it is not difficult to understand why the emf in experiment is smaller concerning the specific orientations of Li_2O_2 crystals formed during cell operation as well as the existence of small amount of solvated Li_2O_2 in the solvents. Actually, OCV of 2.85 V has also been reported in a Li-O_2 battery using LiTFSI-DME electrolyte at room temperature by Viswanathan *et al.*[22] It is reasonable that the real emf value for each Li-O_2 battery could deviate from the ideal value of 2.959 V due to the above two possibilities.

Third of all, Fig. 1a shows a zero OCV hysteresis between the equilibrium voltage of discharge and charge. At the first glance, this is surprised since the reaction paths have been regarded as asymmetry in previous paper[18]. Our results reveal that the product at equilibrium state during discharge and charge is dominated by crystalline Li_2O_2 and unstable intermediate phases formed during the reaction of Li and O_2 do not exist at equilibrium states. This result also means that the voltage gap during galvanostatic discharge and charge or cyclic voltammogram is only originated from kinetics, not from the asymmetrical thermodynamic reaction path, which is different from the conversion reactions such as in MnO anodes and FeF_3 cathode.[29,30]

Fourth of all, since U_{eq} is determined unambiguously, the overpotential during discharge and charge can be calculated from the GITT results. From the beginning to the specific capacity of ~1000

mAh g^{-1} as shown in Fig. 1a, the discharge overpotential does not increase too much and as the capacity increases further up to the end of discharge, the overpotential increases exponentially as shown in Fig. 1b. This relationship is consistent with a diffusion controlled process. It is naturally to presume that the size enlargement of Li_2O_2 particles as indicated by the SEM results (Fig. S1) leads to increase of the transport resistance of Li^+ and O^{2-}. Upon charging, η_{ch} shows also exponentially increase rule as a function of Q as shown in Fig. 1b. This indicates that the mass transport during charging also play key role in the rate determining step. The detailed decomposition process of Li_2O_2 at atomic level is still not clear. It has been reported that Li_2O_2 will decompose either at the contact site with the carbon nanotube[31] or at the edge site of Li_2O_2 based on *in situ* SEM and TEM investigations.[32] In each case, it is no doubt that the particle size of Li_2O_2 is decreased gradually during charge. Therefore, it is not reasonable that the diffusion resistance of Li^+ and O^{2-} in Li_2O_2 particles will increase during charge. The electronic contact of Li_2O_2 particles with electrical conducting medium will become worse gradually with charging, however, that will lead to an Ohmic rule. Therefore, the exponential increase of the overpotential during charge should be caused by other factor related to the mass transport. It has been known that side products such as carbonate species (mostly Li_2CO_3) at the electrolyte/Li_2O_2 interfaces will be formed during charge.[13,15] It is therefore to suggest that the coverage and formation of the side products on Li_2O_2 could be the reason for the diffusion controlled behaviour as shown in Fig. 1b.

As shown in Fig. 1a, the OCVs during charge reach the same value (U_{eq} ~2.85 V) when the charge voltage being smaller than 4.0 V. Above 4.0 V, the OCVs cannot return 2.85 V after 6h relaxation but it can also reach the equilibrium value of ~2.85 V after 24 hours relaxation (Fig. S2). Our previous study revealed that most Li_2O_2 particles could be decomposed as the charge voltage is above 4.0 V.[24b] Above this value, carbonate species become detectable owing to the side reactions.[24b] This result implies further that formation of side products leads to a longer relaxation period for the battery to get equilibrium.

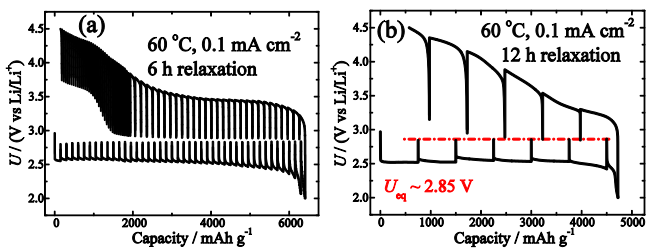

Fig. 2. GITT curves measured at 60°C and the fixed current density of 0.1 mA cm^{-2} with the relaxation time of 6 h (a) and that of 12 h (b).

Fig. 2a shows the GITT curve measured at 0.1 mA cm^{-2} with the same relaxation time (i.e. 6h) as that shown in Fig. 1a. Clearly, with the relaxation time of 6h, the equilibrium voltages for discharge and charge cannot reach the same value. Fig. 2b shows the GITT curve measured at 0.1 mA cm^{-2} with the prolonged relaxation time (i.e. 12 h) in contrast to Fig. 2a. It can be seen that in the case of 0.1 mA cm^{-2} the U_{eq} can also be relaxed to 2.85 V by prolongation of relaxation time. It is known that different current density leads to the Li-O products with different morphology as well as crystallinity,[33] which is also confirmed by the SEM results as shown in Fig. S5. This may lead to different relaxation kinetics in processes of Li_2O_2 growth and decomposition. The fact that the U_{eq} is not significantly dependent on the current density after the sufficient relaxation is further supported by investigations of GITT curves measured at other current densities, as shown in Fig. S6. These results clearly indicate that the Li_2O_2 crystals with the same surface energy can be eventually formed meanwhile with the approximately same values of U_{eq}.

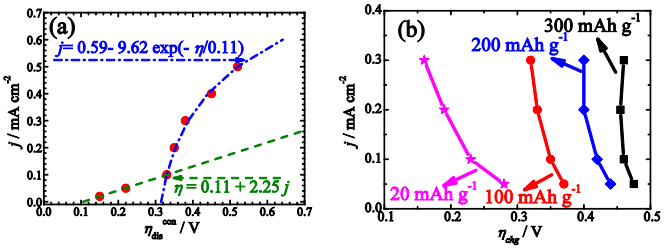

Fig. 3. (a) Current density (j) versus constant discharge overpotential (η_{dis}^{con}) and (b) current density (j) versus η_{chg} at the charge capacities of 20 mAh g^{-1}, 100 mAh g^{-1}, 200 mAh g^{-1}, and 300 mAh g^{-1} (The data are derived from the GITT curves measured at 60°C). The dash curves in 3(a) are simulated curves.

As U_{eq} is known accurately from the GITT curves measured at the different current densities, the values of discharge and charge overpotentials and relationship between overpotential and applied current density can be obtained accordingly. Fig. 3a shows the dependence of η_{dis} on the current density j. It can be seen that the results obey the linear Ohmic law when the current density is less than 0.1 mA cm^{-2}. This is consistent with the fact that the transport of electrons in the electrode and ions in the electrolyte control the reactions. Then an exponential relationship can be seen when the current density is above 0.1 mA cm^{-2}. This is in agreement with a typical diffusion-limited charge-transfer polarization behaviour. Both behaviours can be simulated well, as shown in Fig. 3a. At high current density, it is reasonable to believe that the diffusion of oxygen will become the rate determining step. It is interesting to find that the transition from Ohmic polarization to the diffusion limited charge transfer polarization at the current density of 0.1 mA cm^{-2} seems a first-order transition in our battery. The reason behind that is not clear. It might be related to the variation of the particle size or morphology when the current density changes as discussed above. This needs further clarification.

As shown in Fig. 1 and Fig. 2, the overpotential increases continuously upon charging. The analysis of η_{ch} cannot be done similarly to that of η_{dis}. Therefore, the overpotential values at certain charging depth but different current densities are compared and drawn in Fig. 3b. It is worth noting that the η_{ch} decreases with increasing j in the measured current density range. In the case of the small charge capacity (e.g. 20 mAh g^{-1}) the decreasing amplitude is much larger than that in the case of large charge capacity (e.g. 200 or 300 mAh g^{-1}). This abnormal relationship means that the status of the cathode occur a significant variation during charge. Since the overpotential for charging shows a diffusion controlled behavior, it is plausible that the morphology and particle size of Li_2O_2 and side product are influenced by the current density.[13,34]

Normally, the overpotential should increase when the current density increases. Two issues should be mentioned here. Firstly, in the case of Li-O_2 batteries, as shown in our GITT results as well as other galvanostatisitic experimental, the overpotential increases during charging although Li_2O_2 decompose gradually. As explained above, formation of another high resistive species accompanies with the decomposition of Li_2O_2, leading to increase of the overpotential during charging. In addition, we notice that the overpotentials for the GITT measurements at the smaller current densities are higher than that measured at the larger current densities. It is reasonable that the morphology of Li_2O_2 is influenced by the current densities. At the

larger current density as shown in Fig. S5, the particle size of Li_2O_2 is smaller. Due to the particle size effect of Li_2O_2 and the formation of high resistive unidentified species (most properly Li_2CO_3), the overpotential shows abnormal behaviours, as shown in Fig.3b.

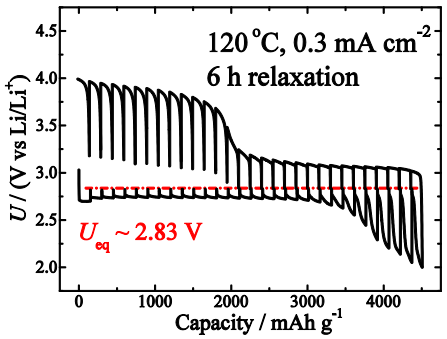

Fig. 4. GITT curves measured at 120°C and the fixed current density of 0.3 mA cm^{-2} with the relaxation time of 6 h.

Table 1. Equilibrium voltage (U_{eq}), discharge overpotential (η_{dis}), charge overpotential (η_{ch}) at 100 mAh g^{-1} for the batteries measured at 0.3 mA cm^{-2} for different temperatures (T).

T (°C)	U_{eq} (V)	η_{dis} (V)	η_{ch} (V) at 100 mAh g^{-1}
60	2.850	0.390	0.320
80	2.842	0.218	0.309
100	2.835	0.142	0.255
120	2.830	0.100	0.170

Temperature is another factor to influence the thermodynamic and kinetic properties. GITT measurements at different temperatures including 60°C, 80°C, 100°C and 120°C were carried out with the same current density of 0.3 mA cm^{-2} and the same relaxation time of 6h. The GITT curves for 60°C and 120°C are shown in Fig. 1a and Fig. 4, respectively. Those for two other temperatures are shown in Fig. S7. On basis of these curves, the values of U_{eq}, η_{dis}, η_{ch} (100 mAh g^{-1}) are calculated and summarized in Table 1. As shown in Fig. S3 clearly, this battery shows a negative temperature coefficient of -62.6 J·mol^{-1}·K^{-1}.

The elevated temperature greatly decreases the overpotentials for both discharge and charge. At 120°C, the η_{dis} and η_{ch} (100 mAh g^{-1}) are 0.10 V and 0.17 V, respectively, compared to 0.39 V and 0.32 V at 60°C. This result indicates that the increase of temperature is an effective means to reduce the battery overpotentials.

According to Ref. [22], the current density as a function of the overpotential for discharge or charge can be written as

$$j \propto -[Li^+]O_2^* exp\left(-\frac{\Delta G_0^{\pm}}{k_B T}\right) exp\left(\frac{\alpha e \eta}{k_B T}\right) \quad (6)$$

where $[Li^+]$ and O_2^* are the reactant at or near the surface, $\Delta G_0^{\pm}$ is the kinetic barrier to the limiting reaction at the equilibrium potential, α is the symmetry factor, and e is the charge on the electron. Based on the data listed in Table 1, the $\Delta G_o^{\pm}/\alpha$ values for discharge and charge can be estimated to be 1.99 and 1.15 eV, respectively. If assuming $\alpha \approx 0.5$, this yields a barrier of ~1.0 eV for discharge and ~0.58 eV for charge at 100 mAh g^{-1}.

As shown in Fig. 4, a semi-plateau of charge voltage appears around 4.0 V. In comparison to Fig. 1, it seems that the temperature increase from 60°C to 120°C makes this plateau behaviour more obvious. As discussed above, this region corresponds to the side-product reaction, which is enhanced by the elevated temperature. This information is consistent with that reported for MPP-TFSI-based cells,[35] the details of which will be presented in the forthcoming paper.

Conclusions

GITT measurements have been carried out on the Li-O_2 batteries at different current densities as well as different temperatures. Several conclusions can be drawn:

1) OCV of Li-O_2 battery at 60°C is 2.850 V in the observed cell;
2) The Li-O_2 battery shows a negative temperature coefficient of-62.6 ($-3.25\times10^{-4}nF$, with n = 2) J·mol^{-1}·K^{-1}, accordingly, the emf of Li-O_2 battery at 25°C should be 2.861 V;
3) The thermodynamic equilibrium voltage gap between charging and discharging is zero;
4) Overpotential increases exponentially during discharging under constant current density and the relationship between overpotential and current density obeys the linear Ohmic law when the current density is smaller than 0.1 mA cm^{-2} and the exponential relationship when the current density is above 0.1 mA cm^{-2}.
5) During charging at the fixed current density (i.e. galvanostatic charging), the size effect of Li_2O_2 and the formation of high resistive unidentified species (most probably Li_2CO_3) might be responsible for the anomalous relationship between the overpotential and the current density.
6) Elevating temperature from 60°C to 120°C can decrease the voltage gap from 0.71 V to 0.27 V.

Overall, a number of issues related to the thermodynamic and kinetic behaviours as aforementioned have been raised by the GITT technique here. For more and deeper understanding, investigations based on the GITT in combination with other techniques such as electrochemical impedance spectroscopy (EIS), potentiostatic intermittent titration technique (PITT) and *in situ* X-ray absorption spectroscopy (XAS) are underway in our lab.

Acknowledgements

The authors would thank the financial supports from the National Key Basic Research Program of China 2014CB921004, Key Project of the Chinese Academy of Sciences under Grant No. KGZD-EW-202-2, NSFC (51325206) and the Science Foundation for Youth Scholar of State Key Laboratory of High Performance Ceramics and Superfine Microstructures (SKL201303).

Notes and references

[a] State Key Laboratory of High Performance Ceramics and Superfine Microstructure, Shanghai Institute of Ceramics, Chinese Academy of Sciences, Shanghai 200050, China.
[b] Institute of Physics, Chinese Academy of Sciences, Zhongguancun South 3rd Street No. 8, Beijing 100190, China.
* Corresponding author: xxguo@mail.sic.ac.cn.

† Electronic Supplementary Information (ESI) available: Experimental methods and Fig. S1 to S7 are given. See DOI: 10.1039/c000000x/.

1 K. M. Abraham, Z. Jiang, *J. Electrochem. Soc.* 1996, **143**, 1.
2 G. Girishkumar, B. McCloskey, A. C. Luntz, S. Swanson, W. Wilcke, *J. Phys. Chem. Lett.* 2010, **1**, 2193.
3 P. G. Bruce, S. A. Freunberger, L. J. Hardwick, J. M. Tarascon, *Nat. Mater*. 2012, **11**, 19.

4 Y. Y. Shao, F. Ding, J. Xiao, J. Zhang, W. Xu, S. Park, J.-G. Zhang, Y. Wang, J. Liu, *Adv. Funct. Mater*. 2013, **23**, 987.
5 Y. -C. Lu, D. G. Kwabi, K. P. C. Yao, J. R. Harding, J. Zhou, L. Zuin, Y. Shao-Horn, *Energy & Environ. Science* 2011, **4**, 2999.
6 R. Black, B. Adams, L. F. Nazar, *Adv. Energy Mater.* 2012, **2**, 801.
7 H. –G. Jung, J. Hassoun, J. –B. Park, Y. –K. Sun, B. Scrosati, *Nat. Chem.* 2012, **4**, 579.
8 Z. Peng, S. A.Freunberger, Y. Chen, P. G. Bruce, *Science* 2012, **337**, 563.
9 J. Lu, Y. Lei, K. C. Lau, X. Luo, P. Du, J. Wen, R. S. Assary, U. Das, D. J. Miller, J. W. Elam, H. M. Albishri, D. A. El-Hady, Y.-K. Sun, L. A. Curtiss, K. Amine. *Nat. Commun.* 2013, **4**, 2383.
10 J. J. Xu, Z. L. Wang, D. Xu, L. L. Zhang, X. B. Zhang, *Nat. Commun.* 2013, **4**, 2438.
11 H.-D. Lim, K.-Y. Park, H. Song, E. Y. Jang, H. Gwon, J. Kim, Y. H. Kim, M. D. Lima, R. O. Robles, X. Lepró, R. H. Baughman, K. Kang, *Adv. Mater*. 2013, **25**, 1348.
12 K. Takechi, S. Higashi, F. Mizuno, H. Nishikoori, H. Iba, T. Shiga, *ECS Electrochem. Lett.* 2013, **1**, A27.
13 R. Black, J.-H. Lee, B. Adams, C. A. Mims, L. F. Nazar, *Angew. Chem. Int. Ed.* 2013, **52**, 392.
14 Z. Jian, P. Liu, F. Li, P. He, X. Guo, M. Chen, H. Zhou, *Angew. Chem. Int. Ed.* 2014, 53, 442.
15 (a) X. X. Guo, N. Zhao, *Adv. Energy Mater.* 2013, 3, 1413; (b) N. Zhao, C. L. Li, X. X. Guo, *Energy Technol.* 2014, **2**, 317.
16 H.-D. Lim, H. Song, J. Kim, H. Gwon, Y. Bae, K.-Y. Park, J. Hong, H. Kim, T. Kim, Y. H. Kim, X. Lepró, R. Ovalle-Robles, H. B. Ray, K. Kang, *Angew. Chem. Int. Ed.* 2014, **126**, 4007.
17 I. Kowalczk, J. Read, M. Salomon, *Pure Appl. Chem.* 2007, **79**, 851.
18 Z. Peng, S. A. Freunberger, L. J. Hardwick, Y. Chen, V. Giordani, F. Barde, P. Novak, D. Graham, J.-M. Tarascon, P. G. Bruce, *Angew. Chem. Int. Ed.* 2011, **50**, 6351.
19 C. O. Laoire, S. Mukerjee, K. M. Abraham, E. J. Plichta, M. A. Hendrickson, *J. Phys. Chem. C* 2010, **114**, 9178.
20 B. D. McCloskey, R. Scheffler, A. Speidel, G. Girishkumar, A. C. Luntz, *J. Phys. Chem. C* 2012, **116**, 23897.
21 S. Y. Kang, Y. Mo, S. P. Ong, G. Ceder, *Chem. Mater.* 2013, **25**, 3328.
22 V. Viswanathan, J. K. Nørskov, A. Speidel, R. Scheffler, S. Gowda, A. C. Luntz, *J. Phys. Chem. Lett.* 2013, **4**, 556.
23 (a) W. Weppner, R. A. Huggins, *J. Electrochem. Soc.* 1977, **124**, 1569; (b) P. L. Taberna, S. Mitra, P. Poizot, P. Simon, J.-M. Tarascon, *Nat. Mater*. 2006, **5**, 567.
24 (a) F. Mizuno, K. Takechi, S. Higashi, T. Shiga, T. Shiotsuki, N. Takazawa, Y. Sakurabayashi, S. Okazaki, I. Nitta, T. Kodama, H. Nakamoto, H. Nishikoori, S. Nakanishi, Y. Kotani, H. Iba, *J. Power Sources* 2013, **228**, 47; (b) Z. H. Cui, W. G. Fan, X. X. Guo, *J. Power Sources* 2013, **235**, 251.
25 D. Zhu, L. Zhang, M. Song, X. Wang, R. Mi, H. Liu, J. Mei, L. W. M. Lau, Y. Chen, *J Solid State Electrochem*. 2013, **17**, 2539.
26 C. X. Zu, H. Li, *Energy & Environ. Science* 2011, **4**, 2614.
27 M. Binnewies, E. Mike, *Thermochemical Data of Elements and Compo unds*, Wiley-VCH, Weinheim, Second, revised and extended edition, 2002.
28 Y. Mo, S. P. Ong, G. Ceder, *Phys. Rev. B* 2011, **84**, 205446.
29 (a) O. Delmer, P. Balaya, L. Kienle, J. Maier, *Adv. Mater.* 2008, **20**, 501; (b) K. Zhong, B. Zhang, S. Luo, W. Wen, H. Li, X. Huang, L. Chen, *J. Power Sources* 2011, **196**, 6802.
30 (a) Z. H. Cui, X. X. Guo, H. Li, *Electrochim. Acta* 2013, **89**, 229; (b) R. E. Doe, K. A. Persson, Y. S. Meng, G. Ceder, *Chem. Mater*. 2008, **20**, 5274.
31 L. Zhong, R. R. Mitchell, Y. Liu, B. M. Gallant, C. V. Thompson, J. Y. Huang, S. X. Mao, Y. Shao-Horn, *Nano Lett.* 2013, **13**, 2209.
32 H. Zheng, D. Xiao, X. Li, Y. Liu, Y. Wu, J. Wang, K. Jiang, C. Che, L. Gu, X. Wei, Y.-S. Hu, Q. Chen, H. Li, *Nano. Lett.* 2014, **14**, 4245.
33 B. D. Adams, C. Radtke, R. Black, M. Trudeau, K. Zaghib, L. F. Nazar, *Energy & Environ. Science* 2013, **6**, 1772.
34 B. M. Gallant, R. R. Mitchell, D. G. Kwabi, J. Zhou, L. Zuin, C. V. Thompson, Y. Shao-Horn. *J. Phys. Chem. C* 2012, **116**, 20800.
35 B. D. McCloskey, D. S. Bethune, R. M. Shelby, T. Mori, R. Scheffler, A. Speidel, M. Sherwood, A. C. Luntz, *J. Phys. Chem. Lett.* 2012, 3, 3043.